

Bond analysis of cobalt and iron based skutterudites: elongated lanthanum bonds in $\text{LaFe}_4\text{P}_{12}$

Espen Flage-Larsen, Ole Martin Løvvik, Øystein Prytz and Johan Taftø

Department of Physics, University of Oslo, P O Box 1048 Blindern, NO-0316 Oslo, Norway

E-mail: espen.flage-larsen@fys.uio.no

Abstract. Motivated by the possibility of further improving the thermoelectric properties of skutterudites we investigate charge transfer and bonding in this class of materials using density functional calculations. Results for the CoP_3 , CoSb_3 , $\text{LaFe}_4\text{P}_{12}$ and the hypothetical FeP_3 compounds are presented using the procrystal as the non-binding reference. Spherical integration and Bader analysis are performed to illustrate charge transfer differences between these compounds. The results are in good qualitative agreement with simple electronegativity considerations. The calculations confirm that the transition metal-pnictogen and the pnictogen-pnictogen bonds are covalent, while the filler atom-pnictogen bond is of a more polar and complex nature. The success of the “rattling” cage as phonon inhibitor is explained by a unique semi-correlated bonding scheme between lanthanum and phosphorus. Elongated bonds along the crystal axes surrounds the lanthanum ion and generate a dodecahedra grid. Vibrations along the crystal axes are then closely connected to and scatter from the phosphorus rings. In the other directions, a more uncorrelated vibration is possible. This duality widens the phonon dampening possibilities.

PACS numbers: 61.50.Lt, 63.20.-e, 71.15.Mb, 71.20.Eh, 71.20.Be, 72.10.Di, 72.15.Jf

Submitted to: *New J. Phys.*

1. Introduction

In recent years, skutterudite compounds have attracted much attention as potential thermoelectric materials[1]. This is mainly attributed to their high figure-of-merit[1] and the possibility to substitute and modify the composition while still retaining the basic structure[2]. The figure-of-merit is defined as $ZT = \alpha^2 \sigma T / \kappa$, where α , σ , κ and T are the Seebeck coefficient, the electrical conductivity, the thermal conductivity, and the temperature, respectively. The high ZT value comes as a result of a strong asymmetric density of states around the Fermi energy and the ability to drastically decrease the thermal conductivity by adding interstitial atoms. These structures are also interesting from a physical point of view due to superconducting[3, 4], heavy-fermion[5, 6] and ferromagnetic[7] behaviour.

Empty skutterudite compounds in space group $Im\bar{3}$ have the chemical formula MX_3 , where M and X are transition metals and pnictogens, respectively.

It was early suggested[8] that the inclusion of heavy atoms in the open voids, the positions of the filler ions in figure 1, could reduce the thermal conductivity. This idea has since been confirmed by numerous studies[9]. The decrease of the thermal conductivity is attributed to a ‘‘rattling’’ behaviour of the filler atoms, confirmed by inelastic neutron diffraction studies[10].

The true nature of the rattling behaviour has not yet been determined, but it has been suggested that the filler ions can rattle independently[11] in the dodecahedra of X ions. Recent studies[12, 13] contradict this picture and suggest a more correlated motion of the filler atoms.

Changes of the thermal conductivity have also been shown for substitutions in the basic skutterudite framework[14, 15]. Such substitutions can also be tuned to modify the electrical conductivity[16] by influencing the electronic part of the thermal conductivity. Hence both the electrical and thermal conductivity can be tailored by altering the composition. The wealth of different compositions possible in the skutterudite structure has resulted in a number of studies looking for optimal compositions to reach ultimate thermoelectric properties[17, 9]. To assist in the search, an in-depth understanding of the electron structure and lattice thermal conductivity may be helpful.

In this work we focus on the valence electron density and bonding properties. Previous work has indicated the importance of the hybridization between the p- and d-orbitals of the antimonides and transition metals to stabilize the CoSb_6 octahedra[18]. The lowest conduction band responsible for electron transport was furthermore shown to include mainly Sb p-states located in the Sb_4 ring[18]. These rings were also shown to be connected through the CoSb_6 octahedra by the highest valence band. In addition, evidence of delocalized non-bonding Sb s-states was observed.

There has been some discussions[19] as to whether it is the MX_6 octahedra, the X_4 ring or a combination of both[18] that determine the main bonding features of the skutterudite compounds. Numerous studies[20, 21] have calculated and measured the density of states around the Fermi level. From these studies it is quite clear that the

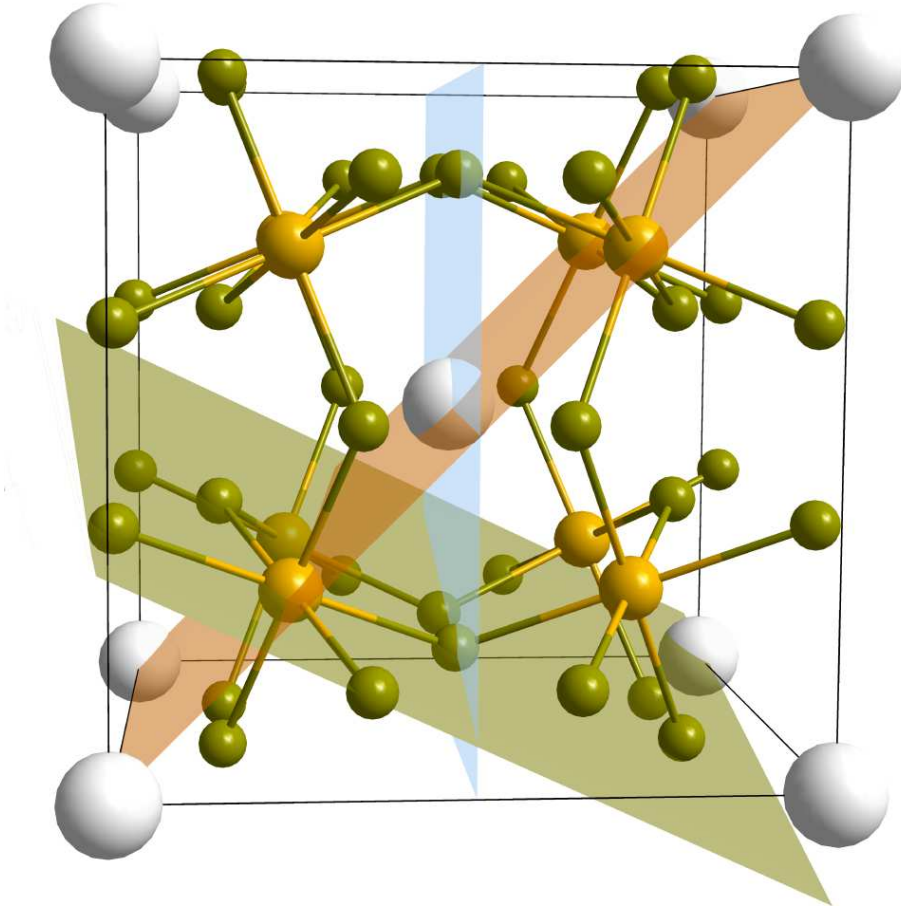


Figure 1. (Color online) The skutterudite structure. Small, medium and large spheres are the pnictogens, transition metals and filler ions, respectively. The octahedral arrangement of pnictogens around the transition metal is shown in addition to the octahedral cutout (green/darkest), the 020 (blue/brightest) and the 110 (red/bright) planes.

3d-states of M lie right under the Fermi level followed by the 3p-states of X , while the X 3s-states lie deep below the Fermi level and are not contributing to any significant bonds. The lower part of the conduction band has primarily 3d- and 3p-state character from M and X respectively.

However, to our knowledge the bonding character of the filler ions has not been specifically addressed in detail beyond what has been suggested in literature reviews[9, 22], in spite of the filler atoms' special role as enhancing lattice thermal resistivity. Recent studies[12, 13] suggest a more correlated movement of the filler atoms. This motivates us to specifically address the filler ion charge transfers.

In this study we investigate the electronic structure and charge transfer in the CoP_3 , CoSb_3 , $\text{LaFe}_4\text{P}_{12}$ and the hypothetical FeP_3 skutterudites. We give an introduction to the DFT and charge transfer calculations in section 2.1 and section 2.2, respectively. Results and discussions follow in section 3 where we briefly list the relaxed structure in

section 3.1 followed by a charge transfer reference discussion in section 3.2. Results of a qualitative charge transfer analysis using the procrystal as a reference are presented in section 3.3 followed by a more quantitative analysis in section 3.4, which cover both estimates of charge depletion numbers and Bader analyses. Brief discussions finally ends section 3. Concluding remarks are given in section 4

2. Computational details

2.1. Density functional theory

The electronic structure and bonding information are ultimately manifested in the charge density, the fundamental quantity in density functional theory (DFT)[23, 24]. This makes DFT an obvious choice for charge density analysis. We have performed DFT calculations in the generalized gradient approximation (GGA)[25, 26, 27, 28] using Perdew-Burke-Ernzerhof (PBE)[29] exchange-correlation functional to obtain the charge density. The highly efficient projector-augmented-wave (PAW)[30, 31] method was also used. All calculation were done using the Vienna Ab initio Simulation Package (VASP)[31, 32, 33, 34, 35, 36].

Crystal structures were relaxed with regards to cell size, shape and atomic positions using the residual minimization scheme, direct inversion in the iterative subspace (RMM-DIIS)[37] algorithm. After the relaxation another self-consistent calculation has been done to ensure correct representation of the system. An energy cutoff of 800 eV for $\text{LaFe}_4\text{P}_{12}$ and 550 eV for CoP_3 and CoSb_3 were necessary to obtain convergence of the total energy to within 2 meV. A k-point grid of $8 \times 8 \times 8$ for the conventional (cubic) unit cell was sufficient to achieve similar convergence.

Comparable smearing conditions are very important during charge analysis, since different smearing parameters will affect the charge density well above errors introduced in the post-processing. A Gaussian smearing[38] of 0.3 eV was sufficient to converge all structures and atoms to 1 μeV within fifty electron steps. The difference between Gaussian and higher order Methfessel and Paxton smearing[39] was found to be very small for $\text{LaFe}_4\text{P}_{12}$, thus Gaussian smearing was used in all cases. Procrystal electron densities for charge transfer analysis were generated from free atom densities obtained from large single atom unit cell calculations using VASP. The lattice constants were scaled two times that of the crystal to avoid any bonding with mirror images. To make sure that the resolution was comparable for the augmentation charges, the grid size was adjusted accordingly.

2.2. Charge transfer analysis

The charge transfer ρ_b in a material can be defined by

$$\rho_b = \rho_0 - \rho_r, \tag{1}$$

where ρ_r is a reference density and ρ_0 is the crystal charge density of the material. Bonding properties can then be quantified and visualized from ρ_b . The choice of ρ_r is important and is discussed in section 3.2

The charge density in three dimensions is difficult to present without the use of proper visualization tools. In this work the charge density is represented by interionic line extractions of the charge density using modified Shepard interpolation[40] or by a scalar contour plot in the planes defined in figure 1. The interpolation routine is used to force correct extraction exactly along the line.

The problem of assigning quantitative charge to an ion and thus determine electron transfer is well known, and a number of different approaches are being used[41]. In this work we will use a Bader analysis[42] scheme to determine the quantitative ionic electron occupancy numbers. The underlying principle of the Bader analysis is based on a division of charge surfaces where the gradient of the charge density does not have a component normal to its surface. Recently Bader analysis has been implemented efficiently[43, 44, 45] in a freely available code[46]. The Bader analysis can sometimes be difficult to interpret and a correct representation of the core charges is necessary.

As an alternative, to determine the charge depletion it is possible to simply integrate the charge density around a single ion inside a sphere. This raises two fundamental objections. In general the bonds are not spherically symmetric. Also, the unit cell volume can not be covered by spheres alone, which means that parts of the electron density must escape the analysis. Nevertheless a spherical body shape is simple to define and intuitively easy to analyse. In this work we have therefore used the spherical integration technique as an alternative to calculate the depletion around each ion, well aware of its limitations. For spherical calculations the radial cutoffs are crucial to obtain representative depletion numbers. A common approach is to use the covalent radius as a the cutoff radius. This is obviously a simplification and may be unreasonable for bonds not obeying covalency.

In this work we suggest an alternative way to determine the radial-cutoff r_d . We start by integrating the charge density difference ρ_b from which information about the charge transfer is directly available. We define the integral I_b as

$$I_b(r_{max}) = \int_{\Omega} \int_0^{r_{max}} \rho_b dr d\Omega, \quad (2)$$

where the volume of integration is limited by the outer radius cutoff r_{max} . The angle dependence is handled by $d\Omega$. The electron charge depletion number Δn_d is now defined as follows

$$\Delta n_d = I_b(r_{max} = r_d). \quad (3)$$

In this work r_d is defined as the radius where the integral I_b peaks. More specifically as

$$\left. \frac{\partial I_b}{\partial r_{max}} \right|_{r_{max}=r_d} = 0. \quad (4)$$

We require that $r_d > r_t$, a lower threshold limit. Choosing this threshold limit can be difficult in general. We have found that a value of $r_t = 0.3 \text{ \AA}$ avoids possible

local oscillations close to the core giving rise to local extremal values. Controllable accuracy during the integration has been obtained by the use of a numerical trapezoidal integration scheme. This relies on the modified Shepard interpolation routine which is able to return any given function value after the initialization of the basis functions, thus allowing a correct representation close to the integration limits without severe performance penalties. Furthermore, we have calculated the mean value of the depletion $\langle \Delta n_d \rangle$ by integrating I_b such that

$$\langle \Delta n_d \rangle = \frac{1}{r_d} \int_0^{r_d} I_b(r_{max}) dr_{max}, \quad (5)$$

Typically a small difference between $\langle \Delta n_b \rangle$ and Δn_d indicates an abrupt and short-ranged depletion zone around the ion (the opposite is true for a larger difference). This and the value of r_d give information about the extension of the depletion. An obvious limitation of this method is that occupancy numbers can not be obtained. To compare charge transfer maxima locations and their covalent character we have defined the center of Pauling electronegativity as $\chi^* = \chi_1 / (\chi_1 + \chi_2)$, where χ_1 and χ_2 are the electronegativities of the respective ions.

The need for a correct representation of the all-electron charge density must be emphasized. Due to the compensator charge density[31] the usual charge density obtained from VASP is not the true all-electron charge density. In this work the all-electron charge density has been explicitly regenerated after a pre-converged run, thus removing the problems associated with the compensator charge density. For the Bader analysis the total charge density (valence+core) have been included as a reference to ensure proper determination of the maximum and minimum valence electron density. For all other calculations in this work the separated all-electron valence charge density has been used exclusively.

It should be mentioned that other geometries are easily adopted in this method and work is in the progress to extend the analysis to ionic basins[47] and other body shapes, still using a selected reference charge density.

3. Results and discussion

3.1. Structural relaxation

Experimental lattice parameters and atom positions were used as a start for the structural relaxation. Results were in good agreement with previous experimental measurements[48, 49, 50] and calculations[21]; lattice constants and Wyckoff positions of all relaxed structures were within one percent of the experimental value. In agreement with earlier reports[48, 49, 50], the P_4 ring becomes more quadratic going from CoP_3 to $LaFe_4P_{12}$. For these materials the width to length ratio (ring ratio) is 0.79 and 0.97, respectively. The Sb_4 ring ratio is 0.96 for $CoSb_3$, in agreement with previous experimental work[51].

Increased deviation from quadratic rings between, CoP_3 and $CoSb_3$ are expected

due to the larger atoms dominating influence on the short bond. This increases the two shortest bond lengths, yielding a more quadratic shaped ring.

3.2. Choice of charge transfer reference

The determination of charge transfer is a difficult process due to the choice of charge reference. From a theoretical point of view we can use a procrystal[52] charge density ρ_p . This is generated from a superposition of free atomic charge densities embedded in the crystal unit cell, similar to the independent atom model[53]. These charge densities will overlap, but bonding features are absent. This is intuitive and generality is preserved. The bonding properties can be determined from equation 1 using ρ_p as the reference charge density ρ_r .

Different experimental methods exist to determine the charge density and/or charge transfer. One approach is to compare spectroscopic data with standard state references ρ_m [20, 54, 55, 56]. The relative intensity difference may then be converted to occupancy numbers[57]. A more direct approach is to perform diffraction experiments and refine the structure factors by starting from overlapping atomic orbitals[52, 58, 59]. This reference is in principle equivalent to the procrystal used in this work. The structure-factor refinement is stopped when sufficient agreement with experimental diffraction intensities is reached. A standard state charge density ρ_m reference will already contain bonding features on the reference level.

Comparisons between different compounds are then complicated by the lack of a common bond-free reference. To illustrate the complications we have calculated the spherically integrated charge density difference ρ_b around a M ion for $\text{LaFe}_4\text{P}_{12}$ and CoP_3 using the free atom ρ_a , the standard state ρ_m and the procrystal ρ_p charge density references. Moving from the ρ_p reference to ρ_m a decrease depletion around the M ion is expected due to the underlying bonding features in ρ_m . The charge around an atom in the procrystal can be anticipated to be larger than around the free atom due to the overlapping free atom charge densities. Both are clearly confirmed in figure 2. In the case of $\text{LaFe}_4\text{P}_{12}$ a charge depletion around Fe is observed using both the standard state Fe and the procrystal as references. However, the magnitude and gradient are different between the two references. More serious problems emerge when standard state Co for CoP_3 is used. A charge buildup close to Co ion is then found, opposite to what is seen from the procrystal results. The two references thus represent two different pictures; a buildup and a depletion of charge respectively.

Hence, if we intend to compare charge transfer magnitudes between CoP_3 and $\text{LaFe}_4\text{P}_{12}$ we should preferably use ρ_p or ρ_a as a reference. The procrystal represents a consistent reference in charge transfer analysis, but may be difficult to use directly as a reference experimentally. All further charge transfer analysis in this work use the procrystal ρ_p as the reference charge density ρ_r .

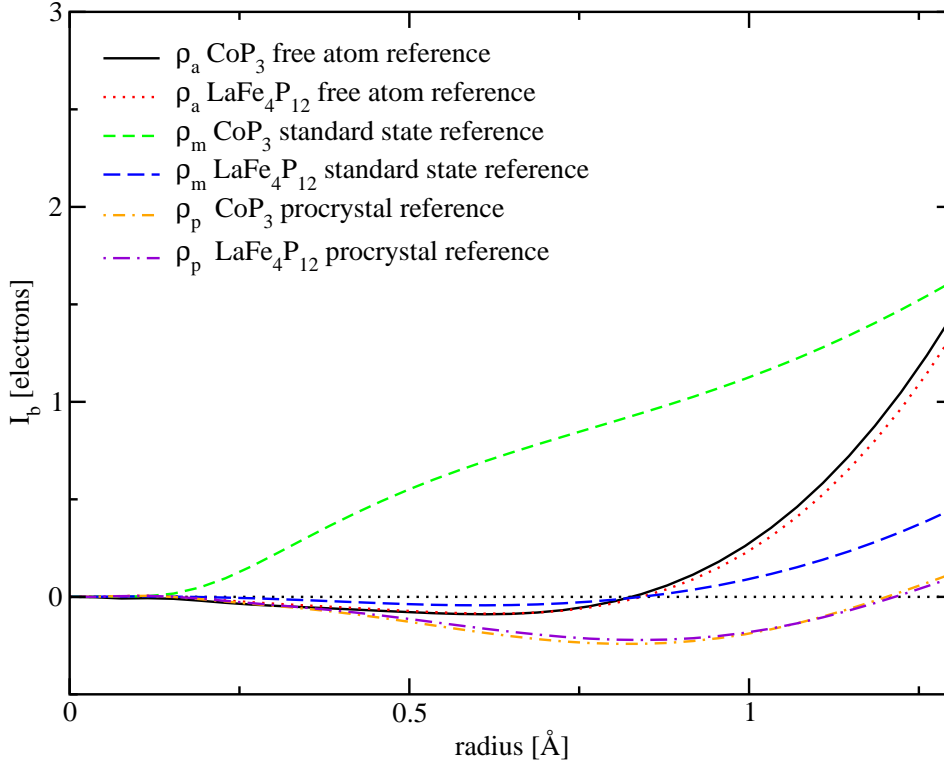


Figure 2. (Color online) The effect of different charge references ρ_r on the integrated charge density difference I_b around the transition metal. References employed are the standard state ρ_m (long-dashed line for $\text{LaFe}_4\text{P}_{12}$, short-dashed line for CoP_3), the atomic ρ_a (dotted line for $\text{LaFe}_4\text{P}_{12}$, solid line for CoP_3) and the procrystal ρ_p (long-dash-dotted line for $\text{LaFe}_4\text{P}_{12}$, short-dash-dotted line for CoP_3).

3.3. Qualitative charge transfer analysis

Charge density differences ρ_b have been calculated for $\text{LaFe}_4\text{P}_{12}$ using the procrystal as a reference, $\rho_r = \rho_p$. Contour plots of ρ_b in the octahedral plane, the plane containing the P_4 ring (020 in-plane shifted) and the plane containing one La ion and four P ions (020) are shown in figure 3, figure 4 and figure 5 respectively. They correspond to the planes illustrated in figure 1. A line is indicated in each contour plane which defines a line extraction of the charge transfer in order to complement the contour plot. The maximum along these lines, their relative distance and the center of electronegativity are listed in table 1.

Due to the lack of core electrons, there is a clear divergent behaviour close to each ion core, but this should not be of importance to the charge transfer analysis presented. The distances have been normalized to a relative distance x in order to facilitate direct comparison between the different compounds.

First of all, a significant charge depletion locally around the Fe ion is clearly observed in figure 3. The charge depletion is directional and facing the P ions, while depletion around the P ions is moderate. Also, a charge buildup between the Fe and P ion is observed in figure 3 with a maximum value and a relative distance listed in table

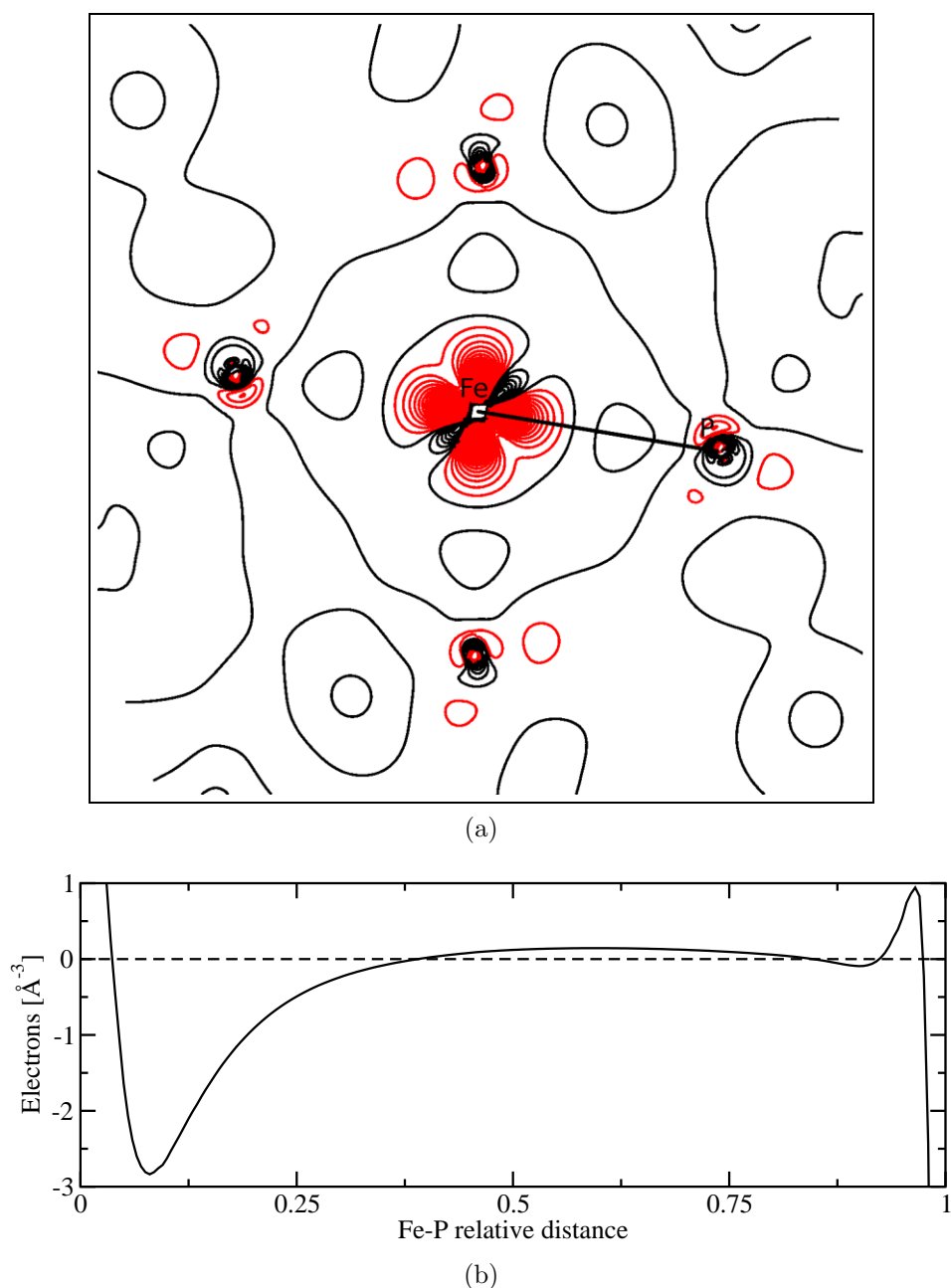


Figure 3. (Color online) (a) Contour plot of the charge density difference ρ_b for $\text{LaFe}_4\text{P}_{12}$ in the octahedra cutout (green/darkest plane in figure 1). Positive charge transfer (black/dark) are drawn from 0 to 1.0 electrons/ \AA^3 , while the negative (red/light) are drawn from -3 to 0 electrons/ \AA^3 . The contour spacing is 0.1 electrons/ \AA^3 . (b) Inter-ionic extraction of ρ_b between Fe and P (indicated by the black line in (a)). The distance is normalized.

1.

Going to the P_4 ring in figure 4, parts of the charge transfer to the Fe-P binding can be seen as four negative lobes around the P ions pointing out of the P_4 ring. These also contribute to the positive P-P charge buildup. It is interesting to note that the charge

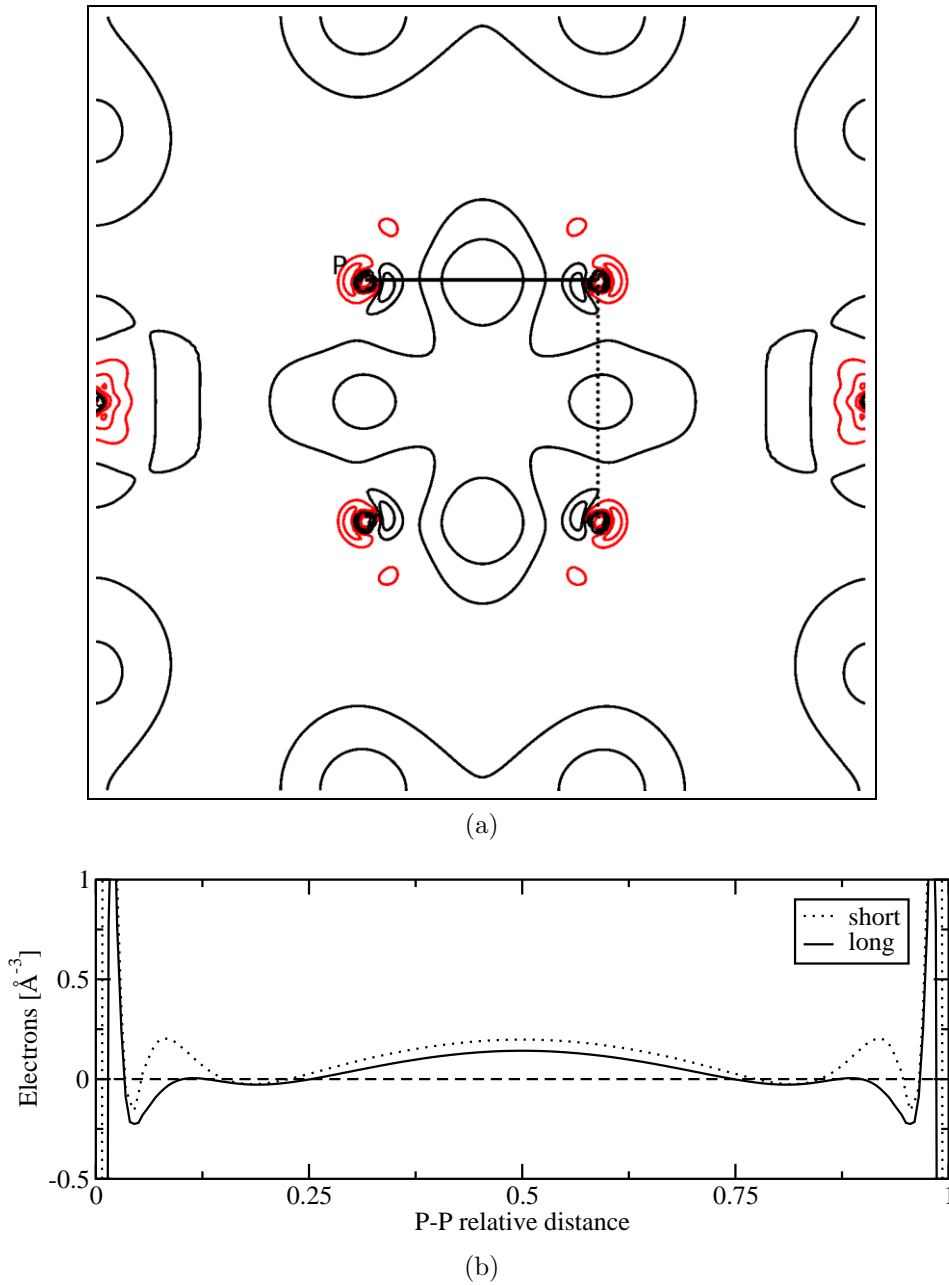


Figure 4. (Color online) (a) Contour plot of the charge density difference ρ_b for $\text{LaFe}_4\text{P}_{12}$ in the plane through the P_4 ring (blue/brightest in figure 1 with a shifted unit cell). Positive charge transfer (black/dark) are drawn from 0 to $2.0 \text{ electrons}/\text{\AA}^3$, while the negative (red/light) are drawn from -0.5 to $0 \text{ electrons}/\text{\AA}^3$, both with a contour spacing of $0.1 \text{ electrons}/\text{\AA}^3$. (b) Inter-ionic extraction of ρ_b between two sets of P ions (indicated by the black lines in (a)). The straight and dotted lines represent the short and long inter-ionic charge transfer extractions P-P in the P_4 ring. These lines are indicated in (a). The distances are normalized.

transfer of the short P-P bond is significantly different from its longer counterpart, demonstrating that the shortest bond is the strongest. As expected the maximum

charge buildup is located in the middle of both the short and long P-P bonds.

The P-La charge transfer is given in figure 5. Compared to the Fe-P bond, a maximum value is observed closer to the La ion. In addition significant charge movement close to the P and La ion is confirmed. The depletion close to the P ion is similar to

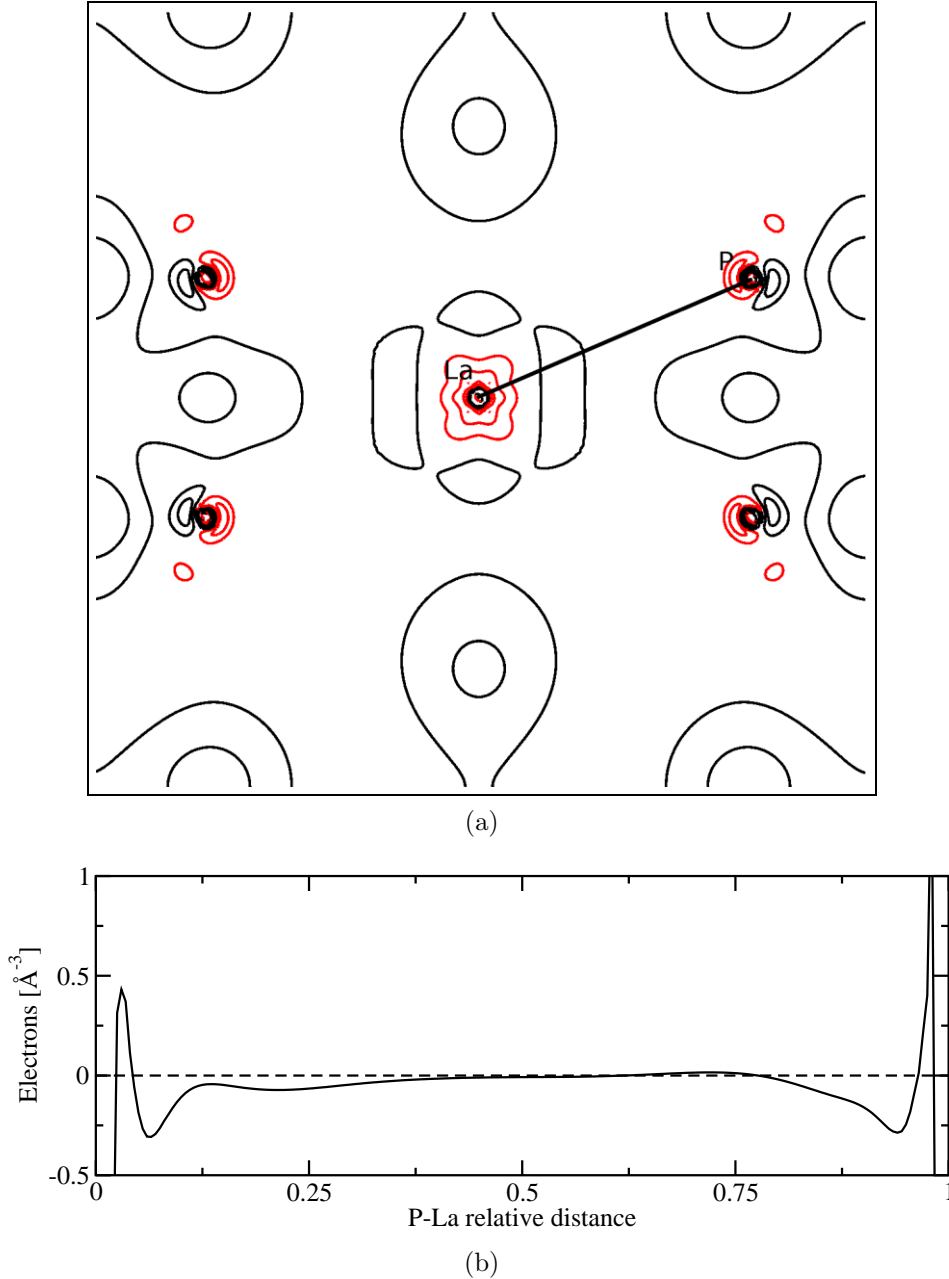


Figure 5. (Color online) (a) Contour plot of the charge density difference ρ_b for $\text{LaFe}_4\text{P}_{12}$ in the plane containing one La surrounded by four P (blue/brightest plane in figure 1). Positive charge transfer (black/dark) are drawn from 0 to 1.0 electrons/ \AA^3 , while the negative (red/light) are drawn from -0.5 to 0 electrons/ \AA^3 , both with a contour spacing of 0.1 electrons/ \AA^3 . (b) Inter-ionic extraction of ρ_b between P and La (indicated by the black line in (a)). The distance is normalized.

the depletion around P for the long P-P bond, which is facing La.

An important question to raise is how much the La ion contributes to the Fe-P charge transfer in $\text{LaFe}_4\text{P}_{12}$ compared to the pure Co to Fe substitution going from CoP_3 to FeP_3 . To illustrate this we have calculated the hypothetical FeP_3 structure based on the atomic positions and unit cell parameters of CoP_3 . The FeP_3 structure was not relaxed. In figure 6 we give the contour plot of the octahedral plane of FeP_3 and the inter-ionic Fe-P line extraction. Comparing figure 3(a) and 6(a) shows that the overall differences between FeP_3 and $\text{LaFe}_4\text{P}_{12}$ in the octahedral plane are small close to the Fe ion, while clear differences are observed in the vicinity of the P ion.

The complete set of relevant charge transfers ρ_b are compared for CoP_3 , CoSb_3 , FeP_3 and $\text{LaFe}_4\text{P}_{12}$ in figure 7 and 8. Maximum values and their relative distances are listed in table 1. In the upper part of figure 7, a charge buildup maxima for CoP_3 and FeP_3 is observed, slightly shifted towards the P ions. Differences between CoP_3 and FeP_3 close to the M ion are also observed, while the differences closer to the P ions are marginal. Close to the M ions the largest charge depletion is found in CoP_3 followed by CoSb_3 , $\text{LaFe}_4\text{P}_{12}$ and FeP_3 . The location of the smallest charge buildup maximum for Co-Sb is in the middle of the M - X bond. In addition a second larger maximum closer to the P ion is observed. This extra maximum is completely lacking for the other compounds.

In the lower part of figure 7, both P-La and M -La inter-ionic charge transfers are illustrated for CoP_3 , FeP_3 and $\text{LaFe}_4\text{P}_{12}$. For CoP_3 and FeP_3 the virtual position of a filler atom (Wyckoff position a) is used for direct comparison of the electron density around this position. The Fe-La charge transfer in $\text{LaFe}_4\text{P}_{12}$ has three well defined charge difference maxima. The two smallest are about an order of magnitude smaller than the values for the M - X and X - X bonds. The inter-ionic charge transfer extraction between Fe and the virtual La position for FeP_3 follows that of $\text{LaFe}_4\text{P}_{12}$ close to the Fe ion; the largest difference between the two compounds (except the obvious difference close to the La position) is observed in the first peak close to the Fe ion. When La is added, a change in charge depletion close to the P ion in the P-La extraction is observed. However, this depletion is larger for $\text{LaFe}_4\text{P}_{12}$ than FeP_3 , thus signifying a redistribution of charge close the P ion when La is added. A noteworthy observation is the difference between Fe and Co for the M -La bond direction. Close to the Co ion there is a significant charge buildup, which is not so evident close to the Fe ion.

From figure 8 it is clear that the P-P charge transfer changes upon addition of La. A reconfiguration of both the long and short bonds is observed. The charge buildup at the midpoint and close to P decreases when La is added. For the P-P bond in CoP_3 the short to long charge buildup maximum ratio is 0.83. For FeP_3 the ratio is 0.79, while it changes to 0.72 for $\text{LaFe}_4\text{P}_{12}$. Also, when La is added there is a reconfiguration; the short and long P-P distances are exchanged compared to FeP_3 . When turning to the antimonide, the Sb-Sb bond exhibit smaller charge buildup relative to the P-P bond with a short to long charge buildup maximum ratio of 0.91.

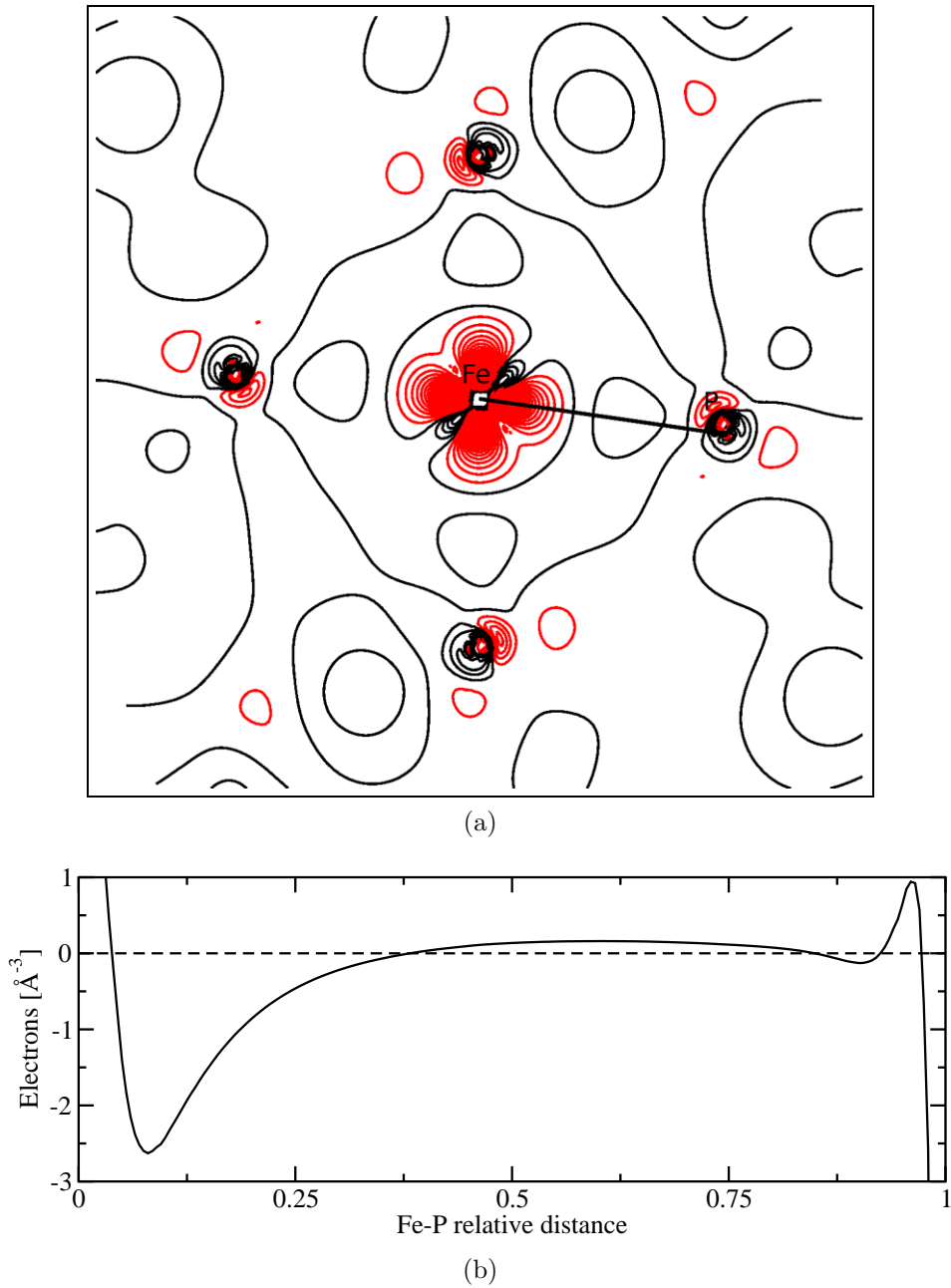


Figure 6. (Color online) (a) Contour plot of the charge density difference ρ_b for FeP_3 in the octahedra (green/darkest plane in figure 1). Positive charge transfer (black/dark) are drawn from 0 to 1.0 electrons/ \AA^3 , while the negative (red/light) are drawn from -3 to 0 electrons/ \AA^3 , both with a contour spacing of 0.1 electrons/ \AA^3 . (b) Inter-ionic charge extraction of ρ_b between Fe and P (indicated by the black line in (a)). The distance is normalized.

3.4. Quantitative charge analysis

3.4.1. *Charge depletion* In table 2 the spherical charge depletion number Δn_d as defined in equation 3 and its mean value $\langle \Delta n_d \rangle$ defined in equation 5 are given. From this table we observe that the charge depletion number around the M ion is largest in

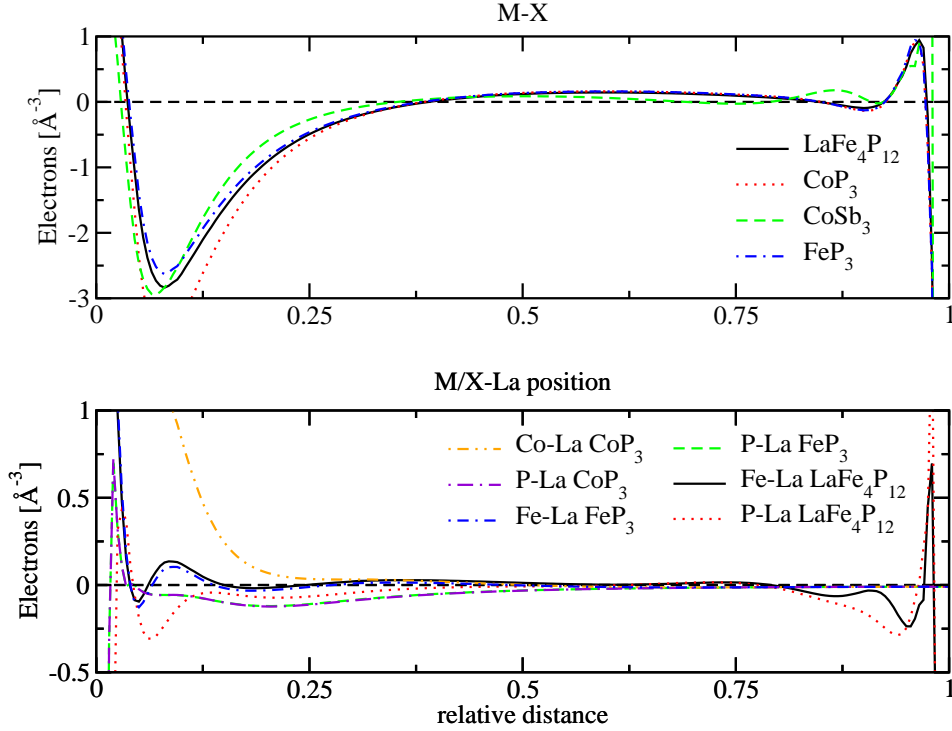


Figure 7. (Color online) Inter-ionic extraction of the charge density difference ρ_b between M - X (upper) and M/X -La(lower). The transition metal Co, Sb and the pnictogens P, Sb are designated M and X , respectively. In the upper a comparison between $\text{LaFe}_4\text{P}_{12}$ (solid line), CoP_3 (dotted line), CoSb_3 (dashed line) and FeP_3 (dashed-dotted line) is given, while in the lower a comparison between Fe-La (solid line) and P-La (dotted line) in $\text{LaFe}_4\text{P}_{12}$, Co-”La” (short dashed-double-dotted line) and P-”La” (long-dashed-dotted line) in CoP_3 , Fe-”La” (dashed-dotted line) and P-”La” (dashed) in FeP_3 is given. ”La” represents Wyckoff position a where e.g. La atoms would have been located. The distances are normalized.

CoP_3 followed by $\text{LaFe}_4\text{P}_{12}$, FeP_3 and CoSb_3 . The analogues sequence for the X ions is CoSb_3 , $\text{LaFe}_4\text{P}_{12}$, CoP_3 and FeP_3 . Similar values of $\langle \Delta n_d \rangle$ for CoP_3 , FeP_3 and $\text{LaFe}_4\text{P}_{12}$ are observed, while it is less for Co and larger for Sb in CoSb_3 compared to the other compounds.

The charge depletion around the La ion is largest of all ions, but its mean value is similar to the ones around Co and Fe. The ratio of the depletion number between Co and Fe is almost the same as the relative valence charge difference between the two atoms. It is also observed that the addition of La increases the Fe and P depletion. The depletion cutoff r_d is comparable for the P ions between CoP_3 , CoSb_3 and FeP_3 , while it increases slightly for $\text{LaFe}_4\text{P}_{12}$. Comparable values are also observed among the Co ions and Fe ions in the respective structures.

3.4.2. Bader analysis While the intuitive spherical integration is bound to fail in systems with complicated charge geometries, the Bader analysis is one of the few techniques with a well defined charge partitioning[42]. Despite the clear definition, it

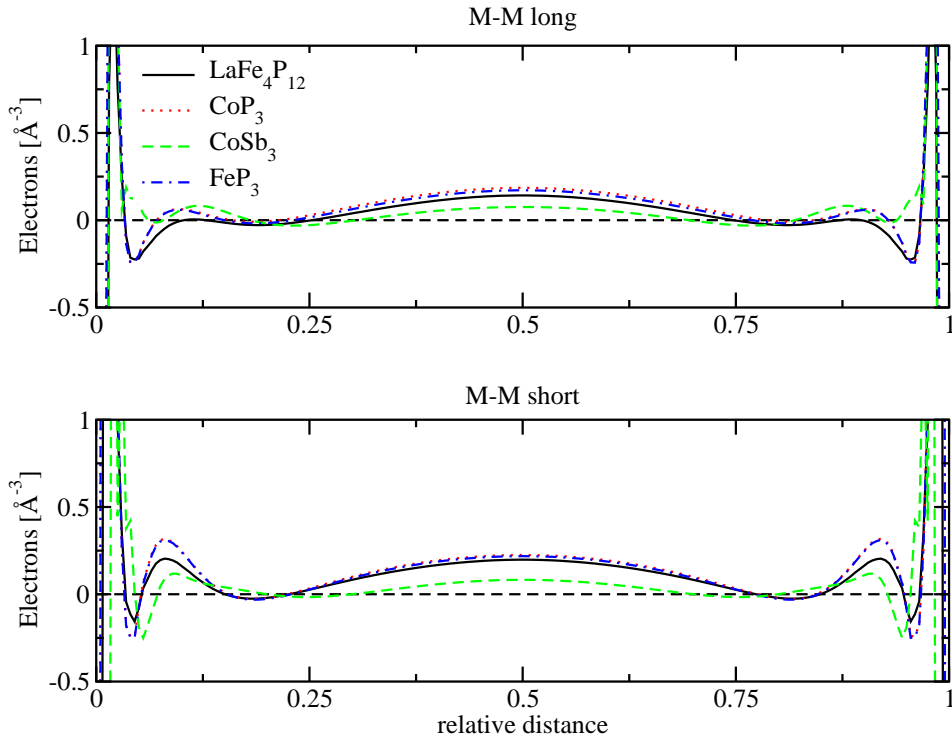


Figure 8. (Color online) Inter-ionic extraction of the charge density difference ρ_b between the short X - X bonds (lower) and its longer counterpart (upper). The pnictogens P and Sb are designated X . A comparison between $\text{LaFe}_4\text{P}_{12}$ (solid line), CoP_3 (dotted line), CoSb_3 (dashed line) and FeP_3 (dashed-dotted line) is given. The distances are normalized.

may be difficult to compare different compounds and their relative charge transfer, due to the variation of the Bader volumes. If the volumes are too different, a comparative charge transfer analysis may be quantitatively unreliable. It is difficult to tell whether the different volumes are due to artifacts of the analysis or different nature of the bonds. Nevertheless, the analysis is well defined and has previously showed to give reliable charges and good comparison conditions even for different volumes. Bader analysis data for CoP_3 , CoSb_3 , FeP_3 and $\text{LaFe}_4\text{P}_{12}$ are given in table 3.

For the X ions four different values are listed corresponding to nonequivalent positions (in the Bader analysis). Even though the differences are small the largest ones are outside estimated error margins. The picture of the charge transfers drawn in the previous sections is confirmed. However, the Bader analysis fails to determine the expected transfer in CoSb_3 , in contrast to previous work[63]. Also, the variation among the antimonides is not present for CoSb_3 . This could indicate a failure of the code used in this work or the Bader analysis itself. The volume filling of the Bader analysis is rather good. The errors for the charge filling of the unit cell is below one percent for most compounds if the average X values are used. However, significant differences are observed confirming the ambiguity of the code used in this work, the core grids or the Bader analysis itself.

Table 1. Charge density difference maxima ρ_{max} and relative distance x for all significant bond directions for CoP_3 , FeP_3 and $\text{LaFe}_4\text{P}_{12}$. In addition the center of Pauling electronegativity χ defined in the text is given (electronegativities are listed in table 1).

		ρ_b^{max} [electrons/ \AA^3]	x	χ^*
CoP ₃	Co-P	0.163	0.6	0.54
	P-P	0.188	0.5	0.5
		0.227	0.5	
FeP ₃	Fe-P	0.160	0.6	0.55
	P-P	0.172	0.5	0.5
		0.218	0.5	0.5
CoSb ₃	Co-Sb	0.086	0.5	0.52
		0.117	0.87	0.52
	Sb-Sb	0.076	0.5	0.5
		0.083	0.5	0.5
LaFe ₄ P ₁₂	Fe-P	0.144	0.59	0.55
	P-P	0.142	0.5	0.5
		0.198	0.5	0.5
	Fe-La	0.167	0.09	0.38
		0.029	0.36	0.38
		0.015	0.74	0.38
	P-La	0.016	0.72	0.33

3.5. Discussion

We will first discuss the character of different bonds. The center of electronegativity χ^* suggests that a charge maximum should occur at 0.54, 0.52 and 0.52 relative distance for the Co-P, Fe-P and Co-Sb bonds if the bonds are purely covalent. From table 1 this is not exactly the case for Co-P and Fe-P bonds, but close enough to conclude that they have a co-ordinated covalent character, in agreement with earlier suggestions[9]. The small deviations are probably attributed to the hybridization set up in the MP_6 octahedra[9]. It is interesting to note that the Co-Sb bond seems to exhibit a stronger covalency than the other $M-X$ bonds, in agreement with previous work[20] and the electronegativity differences. The P-P bonds are obviously covalent in character illustrated by the charge buildup between the ions. It is more complicated to conclude on a Fe-La bond; however, signs of a covalent character is present in this study. The P-La bond does not seem

Table 2. Spherical depletion number Δn_d and their mean value $\langle \Delta n_d \rangle$, the cutoff radii r_d and the Pauling electronegativities[60, 61] χ are shown. The covalent radii r_c [62] are also listed for comparison.

		Δn_d [electrons]	$\langle \Delta n_d \rangle$ [electrons]	r_d [Å]	r_c [Å]	χ
CoP ₃	Co	-0.241	-0.099	0.804	1.260	1.88
	P	-0.048	-0.017	0.803	1.070	2.19
FeP ₃	Fe	-0.218	-0.092	0.841	1.320	1.83
	P	-0.047	-0.016	0.803	1.070	2.19
CoSb ₃	Co	-0.161	-0.067	0.803	1.260	1.88
	Sb	-0.110	-0.046	1.150	1.390	2.05
LaFe ₄ P ₁₂	Fe	-0.221	-0.094	0.841	1.320	1.83
	P	-0.056	-0.020	0.838	1.070	2.19
	La	-0.242	-0.108	1.986	2.070	1.10

to possess a covalent character, in agreement with earlier suggestions[20, 9]. The charge depletion around each ion seems to follow the general trends predicted by simple electronegativity considerations.

The depletion is largest for Co in CoP₃, the structure with ions exhibiting the largest difference in electronegativities (of the unfilled structures). It could be expected from the electronegativities that Fe is more depleted in FeP₃ than Co in CoP₃. But since the Fe atom contains one less electron the relative depletion number is smaller.

In CoSb₃, the difference in electronegativity between M and X is smaller than for CoP₃ and FeP₃. This leads to a decrease of charge depletion around the Co ion and an increase around the Sb ion. From figure 7 an extra charge maximum can be observed close to Sb ion, which is completely lacking in the other compounds. This is probably attributed to the d-electrons in the outer core shell of Sb, which implies a different kind of bond scheme than for P. The peak close to the Sb ion contradicts the previous electronegativity agreements.

The small difference between CoP₃ and FeP₃ confirms that the main differences between the two compounds are found in the vicinity of M .

Iso-surface studies (not shown) also confirm the suggested sp³-like hybridization[9] of P, where the sp³-like lobes are facing P and Fe. For the X - X bonds a greater charge buildup between P than between Sb is observed.

Adding La to FeP₃ increases Fe and P charge depletion, indicating a reorganization of charge to set up of Fe-La and P-La bonds, stabilizing LaFe₄P₁₂ compared to FeP₃.

Table 3. Bader analysis of CoP_3 , FeP_3 , CoSb_3 and $\text{LaFe}_4\text{P}_{12}$. Both the charge and the minimum distance to the Bader surface are given. For the pnictogens all four non-equivalent (in the Bader analysis) values are listed. The charge difference is relative to the formal valence charge of the free atom.

	Atom	valence electrons			Min. distance[Å]
		Atom	Crystal	Difference	
CoP₃					
	Co	9.0	8.89	-0.11	1.02
	P	5.0	5.01	0.01	1.11
			5.04	0.04	1.11
			5.04	0.04	1.13
			5.06	0.06	1.13
FeP₃					
	Fe	8.0	7.78	-0.22	1.00
	P	5.0	5.02	0.02	1.09
			5.07	0.07	1.09
			5.08	0.08	1.12
			5.13	0.13	1.12
CoSb₃					
	Co	9.0	9.32	0.32	1.13
	Sb	5.0	4.88	-0.12	1.34
			4.89	-0.11	1.34
			4.90	-0.10	1.34
			4.91	-0.09	1.34
LaFe₄P₁₂					
	Fe	8.0	7.81	-0.19	1.03
	P	5.0	5.17	0.17	1.13
			5.19	0.19	1.13
			5.19	0.10	1.15
			5.22	0.22	1.15
	La	11.0	9.47	-1.53	1.52

This is also reflected in the differences north and south of the P positions in figure 6 and 3 for FeP_3 and $\text{LaFe}_4\text{P}_{12}$ respectively. A relatively weak binding of La to neighbouring P ions is observed. The maximum charge buildup between La and P is significantly less than what was found in the Fe-P bond (about a tenth). Close to the P ions the setup of a La-P bond and the modification of the P-P bond imply changes in the charge, which is observed. The difference between the X_4 ring ratio of CoP_3 and CoSb_3 is attributed to the increased size of the Sb atoms which will have greater influence on the short bonds.

The results from the Bader analysis generally follow simple electronegativity considerations. This also holds true when La is added to the FeP_3 system. For $\text{LaFe}_4\text{P}_{12}$ the Bader analysis indicates a rather large increase of charge at the P positions, while the charge difference of Fe is similar between FeP_3 and $\text{LaFe}_4\text{P}_{12}$. This is in agreement with the results from the depletion numbers. The different values for the X ions are related to the finite grid resolution. The failure to reproduce physical results for CoSb_3 (the charge transfer behaviour is expected to follow that of CoP_3) is either attributed to the program used in this work, the core grid of Sb or the Bader analysis itself. However, it should be emphasized that within reasonable grid resolutions this behaviour does not change. The core grids and the Bader analysis are not used during the calculation of depletion numbers where such a discrepancy for CoSb_3 is lacking.

Furthermore, the P_4 ring ratio changes quite drastically from CoP_3 to $\text{LaFe}_4\text{P}_{12}$. In CoP_3 the shortest length is facing the vacant filler position, while in $\text{LaFe}_4\text{P}_{12}$ this is opposite. Also, the rectangular P_4 ring in CoP_3 is transformed into a more quadratic shape in $\text{LaFe}_4\text{P}_{12}$ in correspondence with what happens when CoSb_3 is filled with Ce[64]. The La atoms want to bond to the nearby dodecahedra of P ions by redistributing charge from the short P bond to the bond between P and La. This results in a weaker effective P-P bonds close to the La ion, thus increasing the distance between the P ions. As a consequence there is an interchange of the short and long P-P bonds between CoP_3 and $\text{LaFe}_4\text{P}_{12}$.

Adding to the above analysis, differences between M -P bonds in CoP_3 and $\text{LaFe}_4\text{P}_{12}$ are small. There is virtually no difference in the charge buildup except close to the M ion. Thus, the depletion around the Fe ion does not contribute directly in a modified Fe-P binding when La is added, a further evidence of new Fe-La bonds. Due to the similarities close to the Fe ions between FeP_3 and $\text{LaFe}_4\text{P}_{12}$ it is clear that the establishment of P-La bonds would primarily modify the P_4 ring.

From figure 5 elongated charge buildups between the La ion and the long P-P bond is observed. These are aligned along the crystal axes. The bonding between P and La is likely not directional between the ions such that La interacts with the closest P-P bonds by establishing shared states with both P ions. The large depletion cutoff r_d suggest an extended depletion around La. Yet, the elongated bonds are established in this zone, further strengthening the evidence that the La-P bonds are non-directional and elongated. This is highly relevant to the ‘‘rattling’’ behaviour of the filled skutterudites. Vibrations of La along the crystal axes would imply a response from the P dodecahedra and hence be correlated throughout the structure. On the other hand, vibrations along directions between the elongated bond (e. g. in the north-east direction from La in figure 5) are possibly more uncorrelated and anharmonic. Both pictures are supported in previous studies[10, 11, 13, 12] which apparently are contradictory. But we believe that the combination of both pictures is vital for understanding the reduced thermal conductivity. A possible explanation of the phonon dampening in skutterudites is as follows. Take as an example a phonon wave that involves movement of the P_4 ring parallel to the crystal axes. This movement would be transferred onto the elongated

bond, but as lanthanum moves towards the next elongated bond it is deflected towards to openings due to the edged shape of the elongated bond (e. g. moving in the almost north direction from La in figure 5). As a consequence the phonon wave vector is changed and the phonon wave is damped.

4. Conclusions

In this work we have investigated the charge transfer in the CoP_3 , CoSb_3 , $\text{LaFe}_4\text{P}_{12}$ and the hypothetical FeP_3 skutterudite compounds by using the corresponding procrystals as charge references.

It was demonstrated that the alternative references, like the standard state reference, may lead to inconsistent results.

General agreements with simple electronegativity considerations were shown. The covalent character of the $M-X$ and $X-X$ bonds was confirmed, while a slight ionic character was detected for the P-La bond. It was also shown that the addition of La results in a redistribution of charge within the P_4 rings.

A unique bonding scheme between P and La was proposed. We showed that elongated bonds close to the La ion were established when La was added. These elongated bonds were aligned along the crystal axes facing the P_4 ring. Vibrations of the La ion along the crystal axes would then be closely connected with the surrounding P_4 rings. In contrast, vibrations of La along directions between the elongated bonds would be more uncorrelated throughout the structure. The combination yields a quasi-correlated motion of the La ion, which supports recent[12, 13] and previous[10, 11] work. We proposed a possible direct explanation of the phonon dampening in the skutterudites being caused by a change of the phonon wave vector. This change comes as a result of the elongated bonds. Studies are in progress to investigate the spatially resolved movement of La ions to further enlighten this picture.

Acknowledgments

The authors would like to acknowledge support from the Norwegian Research Council and the NOTUR project. In addition we would like to thank Simone Casalo, Ragnhild Sæterli, Ole Bjørn Karlsen and Jon Nilsen for fruitful discussions and ideas.

- [1] G. J. Snyder and E. S. Toberer. *Nature Materials*, 7:105–114, 2008.
- [2] K. Mangersnes, O.M. Løvvik, and Ø. Prytz. *New J. Phys.*, 10:053004, 2008.
- [3] I. Shirovani, T. Uchiumi, K. Ohno, C. Sekine, Y. Nakazawa, K. Kanoda, S. Todo, and T. Yagi. *Phys. Rev. B*, 56:7866, 1997.
- [4] G. P. Meisner. *Physica B*, 108:763, 1981.
- [5] D. A. Gajewski, N. R. Dilley, E. D. Bauer, E. F. Freeman, R. Chau, M. B. Maple, D. Mandrus, B. C. Sales, and A. H. Lacerda. *J. Phys.: Condens. Matter*, 10:6973, 1998.
- [6] D. T. Morelli and G. P. Meisner. *J. Appl. Phys.*, 77:3777, 1995.
- [7] M. E. Danebrock, C. B. H. Evers, and W. Jeitschko. *J. Phys. Chem. Solids*, 57:381, 1996.
- [8] G. A. Slack and V. G. Tsoukala. *J. App. Phys.*, 76:1665, 1994.
- [9] C. Uher. *Semiconductors and semimetals*, 69:139, 2001.

- [10] V. Keppens, D. Mandrus, B. C. Sales, B. C. Chakoumakos, M. B. Maple, D. A. Gajewski, E. J. Freeman, and S. Bennington. *Nature*, 395:876–878, 1998.
- [11] B. C. Sales, D. Mandrus, B. C. Chakoumakos, V. Keppens, and J. R. Thompson. *Phys. Rev. B*, 56:15081, 1997.
- [12] M. M. Koza, M. R. Johnson, R. Viennois, H. Mutka, L. Girard, and D. Ravot. *Nat. Mat.*, 7:805, 2008.
- [13] M. Christensen, A. B. Abrahamsen, N. B. Christensen, F. Juranyi, N. H. Andersen, K. Lefmann, J. Andreasson, C. R. H. Bahl, and B. B. Iversen. *Nat. Mat.*, 7:811, 2008.
- [14] C. Stiewe, L. Bertini, M. Toprak, M. Christensen, D. Platzek, S. Williams, C. Gatti, E. Müller, B. B. Iversen, M. Muhammed, and M. Rowe. *J. Appl. Phys.*, 97:044317, 2005.
- [15] M. Christensen, B. B. Iversen, L. Bertini, C. Gatti, M. Toprak, M. Muhammed, and F. Nishibori. *J. Appl. Phys.*, 96:3148, 2004.
- [16] H. Anno, K. Matsubara, Y. Notohara, T. Sakakibara, and H. Tashiro. *J. Appl. Phys.*, 86:3780, 1999.
- [17] B. C. Sales. *Handbook on the Physics and Chemistry of the Rare Earths*. North Holland, 2003. Invited chapter 211.
- [18] I. Lefebvre-Devos, M. Lassalle, X. Wallart, J. Olivier-Fourcade, L. Monconduit, and J. C. Jumas. *Phys. Rev. B*, 63:125110, 2001.
- [19] M. Lluell, P. Alemany, S. Alvarez, and V. P. Zhukov. *Phys. Rev. B*, 53:10605, 1996.
- [20] A. P. Grosvenor, R. G. Cavell, and A. Mar. *Phys. Rev. B.*, 74:125102, 2006.
- [21] Ø. Prytz, O. M. Løvvik, and J. Taftø. *Phys. Rev. B*, 74:245109, 2006.
- [22] G. S. Nolas, D. T. Morelli, and T. M. Tritt. *Annu. Rev. Mater. Sci.*, 29:89, 1999.
- [23] W. Kohn and L. J. Sham. *Phys. Rev.*, 140:A1133, 1965.
- [24] P. Hohenberg and W. Kohn. *Phys. Rev.*, 136:B864, 1964.
- [25] A. D. Becke. *Phys. Rev. A*, 38:3098, 1988.
- [26] J. P. Perdew, J. A. Chevary, S. H. Vosko, K. A. Jackson, M. R. Pederson, D. J. Singh, and C. Fiolhais. *Phys. Rev. B*, 48:4978(E), 1993.
- [27] J. P. Perdew, J. A. Chevary, S. H. Vosko, K. A. Jackson, M. R. Pederson, D. J. Singh, and C. Fiolhais. *Phys. Rev. B*, 46:6671, 1992.
- [28] D. C. Langreth and M. J. Mehl. *Phys. Rev. B*, 28:1809, 1983.
- [29] J. P. Perdew, K. Burke, and M. Ernzerhof. *Phys. Rev. Lett.*, 77:3865, 1996.
- [30] P. E. Blöchl. *Phys. Rev. B*, 50:17953, 1994.
- [31] G. Kresse and D. Joubert. *Phys. Rev. B*, 59:1758, 1999.
- [32] G. Kresse and J. Furthmüller. *Comp. Mater. Sci.*, 6:15, 1996.
- [33] G. Kresse and J. Furthmüller. *Phys. Rev. B*, 54:11169, 1996.
- [34] G. Kresse and J. Hafner. *Phys. Rev. B*, 49:14251, 1994.
- [35] G. Kresse and J. Hafner. *Phys. Rev. B*, 48:131158, 1993.
- [36] VASP code, <http://cms.mpi.univie.ac.at/vasp>.
- [37] P. Pulay. *Chem. Phys. Lett.*, 73:393, 1980.
- [38] A. De Vita. *PhD Thesis*. Keele University, 1992.
- [39] M. Methfessel and A. T. Paxton. *Phys. Rev. B*, 40:3616, 1989.
- [40] R. J. Renka. *Transactions on Mathematical Software*, 14:151, 1988.
- [41] C. Gatti. *Z. Kristallogr.*, 220:399, 2005.
- [42] R. F. W. Bader. *Atoms in Molecules: A Quantum Theory*. Oxford University Press, New York, 1990.
- [43] W. Tang, E. Sanville, and G. Henkelman. *J. Phys.: Condens. Matter*, 2008. in pres.
- [44] E. Sanville, S. D. Kenny, R. Smith, and G. Henkelman. *J. Comp. Chem.*, 28:899, 2007.
- [45] G. Henkelman, A. Arnaldsson, and H. Jónsson. *Comput. Matter. Sci.*, 36:254, 2006.
- [46] Bader analysis code, <http://theory.cm.utexas.edu/bader/>.
- [47] R. F. W. Bader and C. Gatti. *Chem. Phys. Lett.*, 287:233, 1998.
- [48] T. Schmidt, G. Kliche, and H. D. Lutz. *Acta Crystallogr., Sect. C: Cryst. Struct. Commun.*,

- 43:1678, 1987.
- [49] W. Jeitschko and D. J. Braun. *Acta Crystallogr. B*, 33:3401, 1977.
 - [50] W. Jeitschko, A. J. Foecker, D. Paschke, M. V. Dewalsky, C. B. H. Evers, B. Kuennen, A. Lang, G. Kotzyba, U. C. Rodenwald, and M. H. Moeller. *Z. Anorg. Allg. Chem.*, 626:1112, 2000.
 - [51] A. Ohno, S. Sasaki, E. Nishibori, S. Aoyagi, M. Sakata, and B. B. Iversen. *Phys. Rev. B.*, 76:064119, 2007.
 - [52] L. Wu, Y. Zhu, T. Vogt, H. Su, J. W. Davenport, and J. Taftø. *Phys. Rev. B*, 69:064501, 2004.
 - [53] H. S. W. Massey, E. H. S. Burhop, and H. B. Gilbody. *Electronic and Ionic Phenomena vol. 2*. Clarendon Press, Oxford, 1969.
 - [54] H. Anno, K. Matsubara, T. Caillat, and J.-P. Fleurial. *Phys. Rev. B.*, 62:10737, 2000.
 - [55] J. Graetz, C. C. Ahn, H. Ouyang, P. Rez, and B. Fultz. *Phys. Rev. B.*, 64:235103, 2004.
 - [56] Ø. Prytz, J. Taftø, C. C. Ahn, and B. Fultz. *Phys. Rev. B.*, 75:125109, 2007.
 - [57] D. H. Pearson, C. C. Ahn, and B. Fultz. *Phys. Rev. B.*, 47:8471, 1993.
 - [58] J. M. Zuo. *Rep. Prog. Phys.*, 67:2053, 2004.
 - [59] J. M. Zuo, M. Kim, M. O’Keeffe, and J. C. H. Spence. *Nature*, 401:49, 1999.
 - [60] A. L. Allred. *J. Inorg. Nucl. Chem.*, 17:215, 1961.
 - [61] L. Pauling. *The Nature of the Chemical Bond 3rd ed.* Cornell Univ., USA, 1960.
 - [62] B. Cordero, V. Gómez, M. Revés A. E. Plataro-Prats, Echeverria, E. Cremades, F. Barragán, and S. Alvarez. *Covalent radii revisited*. Dalton Trans., 2008.
 - [63] P. Ghosez and M. Veithen. *J. Phys.: Condens. Matter*, 19:096002, 2007.
 - [64] H. Kitagawa, M. Hasaka, T. Morimura, H. Nakashima, and S. Kondo. *Mater. Res. Bull.*, 35:185, 2000.